

CENTRAL ASIAN JOURNAL OF MEDICAL AND NATURAL SCIENCES
https://cajmns.centralasianstudies.org/index.php/CAJMNS
Volume: 08 Issue: 01 | January 2027 ISSN: 2660-4159

Article

Electrical Conductivity, Dielectric Properties, and Surface Morphology of Polystyrene (PS) Films Doped with ZrO2, MnO2, ZnO, and Al2O3 Nanoparticles

Mustafa Q. Jabbar[1], Raghad M.Omer[2]

1,2. College Of science University of Tikrit , Tikrit , Iraq.
* Correspondence: Mustafa.alobaidi@tu.edu.iq[1], Raghad.m.omar@tu.edu.iq[2]

Abstract: Multiple polystyrene (PS) nanocomposite films embedded with ZrO2, MnO2, ZnO, and Al2O3nanoparticles (NPs) were prepared using the solution casting method. A loading ratio of 0.005 wt.% of the nanoparticles was utilized in film preparation, and the casting process was conducted at room temperature. The electrical and dielectric properties of the PS nanocomposite films were analyzed over a frequency range of (1-3 MHz) using an LCR meter. These parameters included the real and imaginary parts of the dielectric constant (ε' and ε'', respectively), alternating current electrical conductivity "σ" AC , dielectric loss factor (tan"δ"), surface energy loss function (SELF), and volume energy loss function (VELF). All evaluated electrical parameters exhibited significant enhancement upon incorporating the metal oxide NPs compared to the blank PS film. Furthermore, the surface morphology and elemental composition of the PS nanocomposite films were examined using field emission scanning electron microscopy (FESEM) and energy-dispersive X-ray (EDX) spectroscopy. Overall, the findings revealed that PS nanocomposite films demonstrated superior electrical conductivity and dielectric behavior compared to pure PS, making them promising candidates for applications in optoelectronics, microelectronic capacitors, energy storage, and radiation-shielding devices.

Keywords: Polystyrene (PS); PS nanocomposite films; ZrO2, MnO2, ZnO, and Al2O3 nanoparticles; Dielectric constant; Electrical conductivity; Surface morphology.

Citation: Jabbar M. Q., Omer R. M. Electrical Conductivity, Dielectric Properties, and Surface Morphology of Polystyrene (PS) Films Doped with ZrO2, MnO2, ZnO, and Al2O3 Nanoparticles. Central Asian Journal of Medical and Natural Science 2027, 8(1), 101-110

Received: 13th Aug 2026
Revised: 20th Sep 2026
Accepted: 15th Oct 2026
Published: 19th Nov 2026

Copyright: © 2027 by the authors. Submitted for open access publication under the terms and conditions of the Creative Commons Attribution (CC BY) license (https://creativecommons.org/licenses/by/4.0/)

1. Introduction

Polystyrene (PS) is a versatile aromatic thermoplastic polymer that serves as an essential matrix in numerous industrial and technological applications due to its outstanding optical transparency, high chemical resistance, mechanical rigidity, ease of processing, and excellent electrical insulation properties [1]. Structurally, PS consists of long hydrocarbon chains with phenyl groups attached to every alternate carbon atom, making it a non-polar, amorphous polymer with a relatively low dielectric constant ε' = (2.4- 2.6) [2]. Consequently, pure PS is widely utilized in packaging, optical components, and insulating coatings. However, its inherently low electrical conductivity and limited dielectric permittivity restrict its direct utilization in advanced electronic and optoelectronic devices, such as high-energy-density capacitors, sensors, and electromagnetic interference (EMI) shielding.[3]

Composite materials are engineered by combining two or more distinct constituents to achieve superior physicochemical properties that surpass those of the individual components. In particular, polymer nanocomposites—defined as multiphase solid materials where at least one phase has dimensions in the nanometer scale (1-100 nm) have attracted immense scientific interest. Due to their high surface-area-to-volume ratio and quantum confinement effects, inorganic nanofillers interact strongly with polymer chains, modifying the optical band gap, thermal stability, and charge transport mechanisms within the host matrix.

Incorporating semiconducting and high-permittivity metal oxide nanoparticles into a polystyrene matrix provides an effective route to tailor its electrical and dielectric characteristics without compromising its processability [4]. Among various metal oxides, ZrO_2, MnO_2, ZnO, and Al_2O_3 possess unique electronic band structures, high thermal stability, and distinct dielectric responses [5–8]. Specifically, ZrO_2 and Al_2O_3 act as high-k dielectric fillers that enhance charge storage capability, whereas , MnO_2 and ZnO exhibit pronounced semiconducting and pseudocapacitive behaviors that facilitate charge carrier mobility. Dispersing these nanoparticles within the PS matrix introduces localized energy states and enhances interfacial polarization (Maxwell–Wagner–Sillars effect), thereby promoting charge carrier hopping and improving AC electrical conductivity .

In the present work, blank PS and PS nanocomposite films doped with 0.005 wt % of ZrO_2, MnO_2, ZnO, and Al_2O_3 nanoparticles were fabricated via the solution casting technique. The frequency-dependent dielectric constant ($\varepsilon'$and ε''), AC conductivity (σ_{AC}), loss tangent (tanδ), surface energy loss function (SELF), and volume energy loss function (VELF) were systematically investigated in the frequency range of (1-3MHz}. Additionally, FESEM and EDX analyses were performed to evaluate the dispersion quality of the nanoparticles and the morphological modifications across the PS film surfaces.

2. Experimental

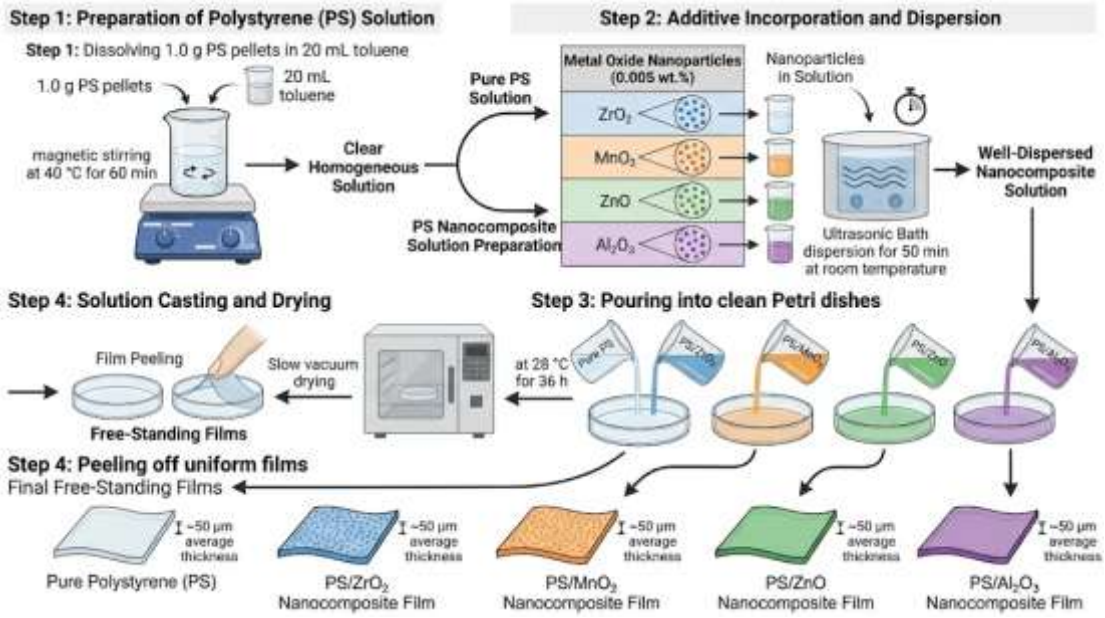
2.1Materials

Commercial-grade polystyrene (PS) pellets with an average molecular weight (Mwt) of (PS 192,000 g /mol) and purity of 99% were obtained from Sigma-Aldrich (Germany). Analytical-grade Toluene (purity 99.5%, Mwt = 92.14g/mol) was supplied by AppliChem (Germany) and used as a solvent without further purification. High-purity nanoparticles of (ZrO_2, MnO_2 ZnO, and Al_2O_3 with average particle sizes of approximately 25.0, 30.0, 20.5, and 40.0nm}, respectively, were purchased from Sigma-Aldrich (Germany). Prior to composite fabrication, the particle sizes and morphologies of the as-received NPs were verified using atomic force microscopy (AFM) .

2.2Preparation of PS/NPs Nanocomposite Films

Pure PS and PS nanocomposite films were fabricated via the standard solution casting method. Initially, (1.0g) of PS pellets was dissolved in (20mL} of toluene under continuous magnetic stirring at (40ºC) for 60 min until a completely clear and homogeneous viscous solution was obtained. Subsequently, a fixed concentration of 0.005 wt.% of each metal oxide ZrO_2, MnO_2, ZnO, and Al_2O_3 was added separately to the PS solutions. To prevent nanoparticle agglomeration and ensure uniform dispersion within the non-polar PS chains, the resulting mixtures were subjected to an ultrasonic bath for 50 min at room temperature.

Finally, the homogeneous mixtures were poured into clean, flat-bottomed glass Petri dishes and left to dry slowly at 28ºC for 36h under vacuum to ensure complete evaporation of the residual solvent. The dried films were carefully peeled off from the glass substrates, yielding uniform, free-standing films with an average thickness of approximately 50μm.



2.3Characterization Techniques

The electrical and dielectric measurements were carried out at room temperature over a frequency range of (1-3 MHz) using an electronic LCR meter (Model 4274A, Hewlett-Packard) to record capacitance (C), inductance (L), and resistance (R). For electrical testing, the blank and nanocomposite PS films were cut into rectangular specimens of dimensions (2 ×1.5 cm) under dry conditions and sandwiched between two silver electrodes to ensure good ohmic contact. Film thickness ($50\mu m$) was precisely determined using a Digital Vernier Caliper (Model 2610 micrometer) .

The surface morphology of the prepared films was inspected using a field emission scanning electron microscope (FESEM, TESCAN MIRA3, Czech Republic) operating at an accelerating voltage of 10 kV. Elemental mapping and chemical composition verification were conducted via energy-dispersive X-ray spectroscopy (EDX) using a Bruker X-Flash 6/10 detector. Optical surface textures were further observed using an optical microscope (MEIJI) equipped with a Lumenera color video camera at 400 × magnification.

3. Results and Discussion

3.1. Dielectric Constant Measurements with LCR Meter

The dielectric behavior of the blank polystyrene (PS) and PS nanocomposite films doped with ZrO_2, MnO_2, ZnO, and Al_2O_3 nanoparticles was investigated as a function of frequency in the range of (1-3 MHz) at room temperature. The complex dielectric permittivity (ε^*) of the nanocomposite systems is expressed in terms of its real and imaginary components according to Equation (1):

$$\varepsilon^*_{(w)}=\varepsilon'_{(w)}-i\varepsilon''_{(w)} \quad \text{.....(1)}$$

where ε' represents the real part of the dielectric constant (associated with electrical energy storage via polarization), and ε'' denotes the imaginary part (associated with dielectric energy dissipation).

3.2 Real and Imaginary Parts of Dielectric Constant (ε' and ε'')

The real part of the dielectric permittivity (ε') for the blank PS and PS/metal oxide nanocomposite films was calculated from the measured capacitance (C) using Equation (2):

$$\frac{C.d}{\varepsilon_o.A}=\varepsilon' \quad \text{.....(2)}$$

where d is the film thickness (50μm), A is the effective area of the silver electrodes (2 × 1.5cm), and ε_0 is the permittivity of free space (8.85 × 10^{-12} F/m), figure 1 showen The real part of dielectric constant (Ɛ') relationship & Log Hz .

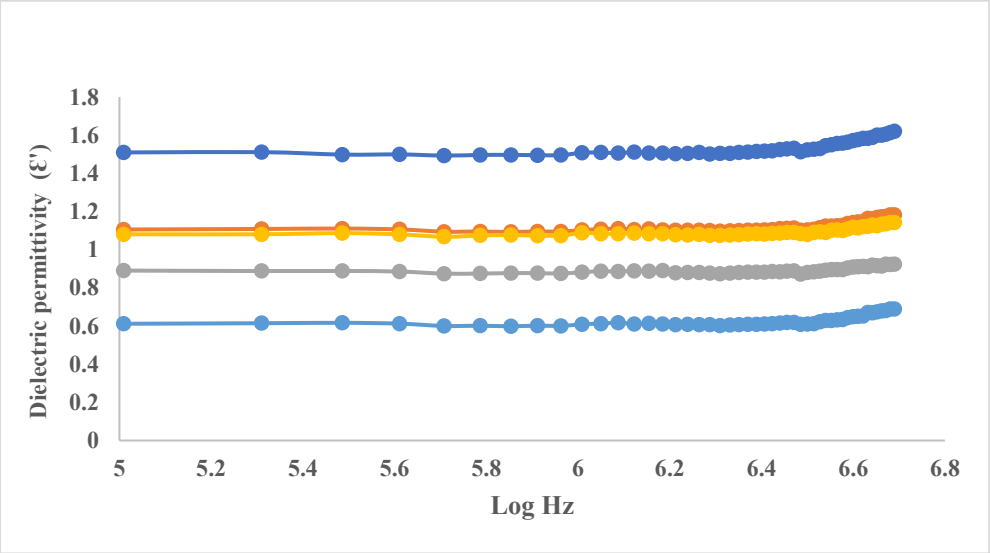


Figure 1. The real part of dielectric constant (Ɛ') relationship & Log Hz

Incorporating 0.005 wt.% of metal oxide nanoparticles significantly increases varepsilon' across the entire frequency spectrum compared to pure PS. This enhancement is attributed to interfacial polarization—known as the Maxwell–Wagner–Sillars (MWS) effect—occurring at the boundaries between the non-polar, insulating PS matrix and the dispersed semiconducting/high-permittivity nanofillers. Among the tested fillers, PS/ZrO_2 and PS/MnO_2 exhibit the highest ε' values due to the inherently high static dielectric constant of (ZrO_2) and the strong space-charge accumulation at the (MnO2/PS interfaces. Furthermore, ε' shows a gradual decrease with increasing logarithmic frequency (log f). At higher frequencies, the permanent and induced dipoles within the PS chains and nanoparticle interfaces fail to reorient rapidly enough to follow the alternating electric field, leading to a reduction in net polarization .

The imaginary part of the dielectric constant ε'') was determined from ε' and the dissipation factor (tanδ) via Equation (3) and figure (2) showen Imaginary part of dielectric permittivity (Ɛ") relationship & Hz

:

$$\varepsilon'' = \varepsilon' \times \tan\delta \quad \text{.....(3)}$$

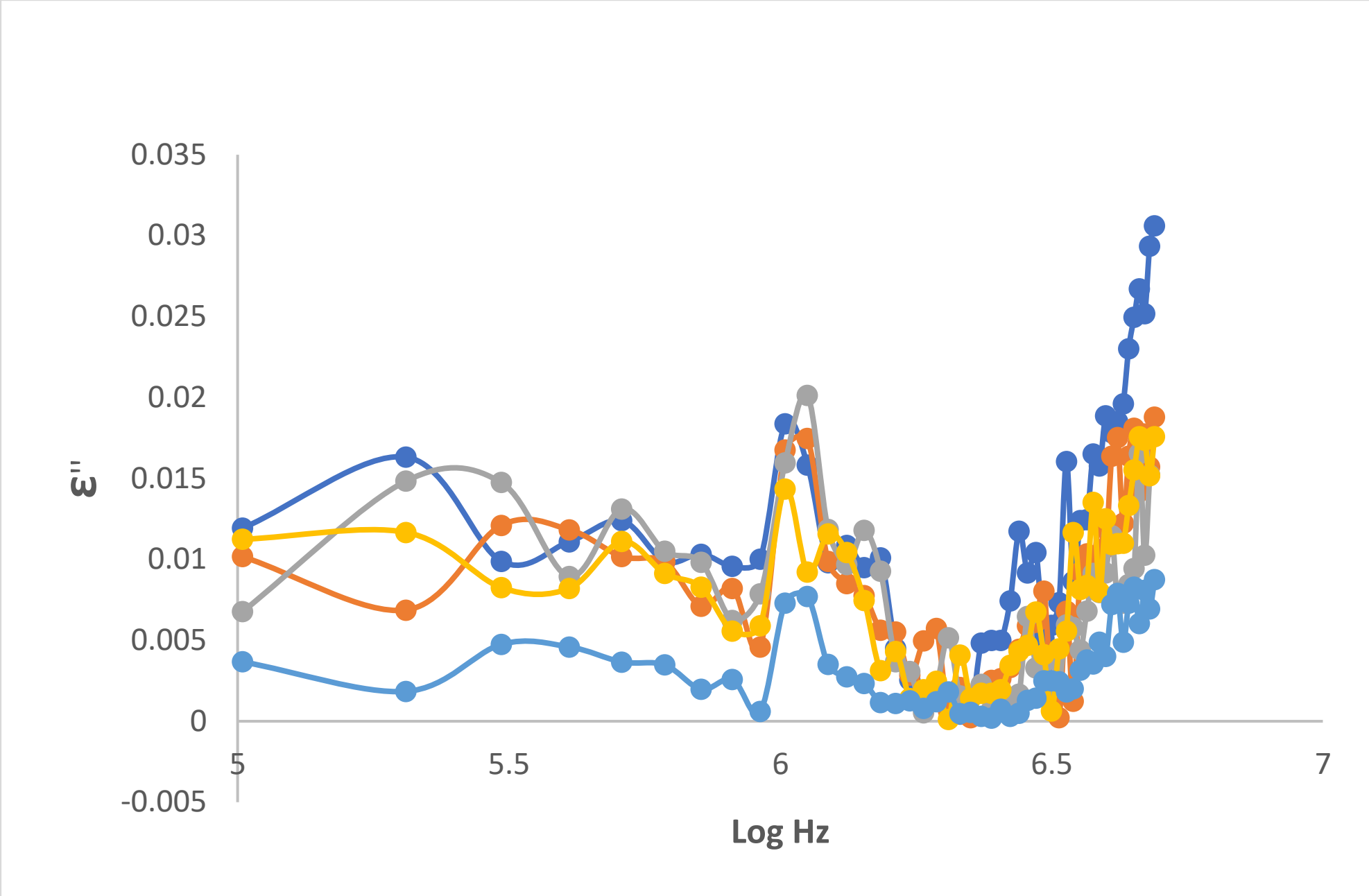


Figure 2. Imaginary part of dielectric permittivity (Ɛ") relationship & Hz

Similar to ($\varepsilon^{'}$, the $\varepsilon^{''}$) values are notably higher for the doped PS films than for the blank PS, and they decline progressively as frequency increases. This decrease at elevated frequencies is ascribed to reduced interfacial polarization losses and diminished dipolar relaxation time within the polymer matrix .

.3.3AC Electrical Conductivity (σ_{AC})

The alternating current electrical conductivity (σ_{AC})of the blank PS and PS nanocomposite films was computed using Equation (4):

$$(\sigma_{AC})=\varepsilon_{\circ}\varepsilon^{'} w\ tan\delta \ldots\ldots\ldots\ldots\ldots\ldots\ldots..(4)$$

where w = $2\pi f$ is the angular frequency and f is the applied frequency,figure (3) shown Conductivity (6) for different nanoparticles of PS nanocomposite films in different frequencies at room temperature.

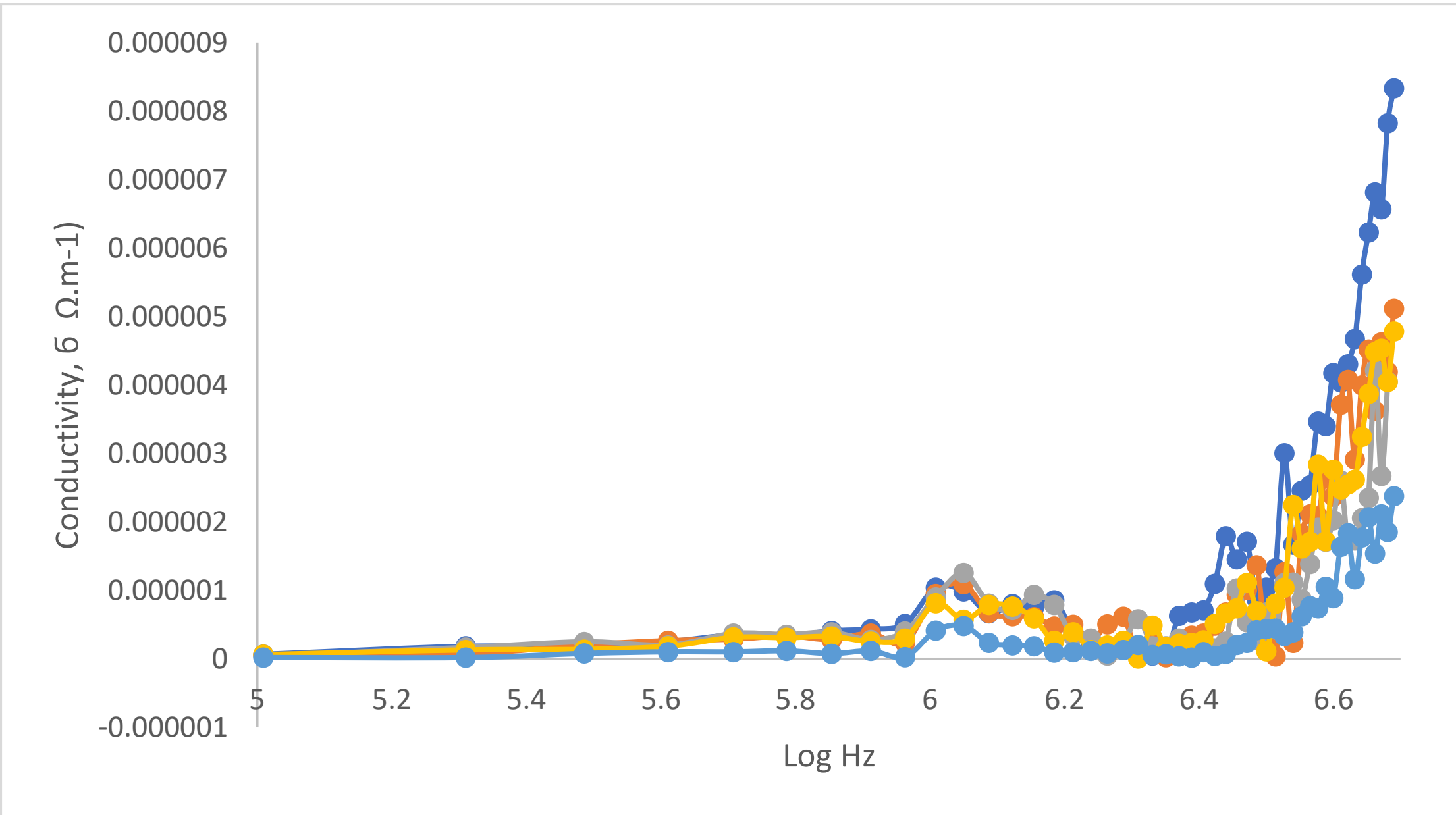


Figure 3. Conductivity (6) for different nanoparticles of PS nanocomposite films in different frequencies at room temperature.

Dispersing ZrO_2, MnO_2, ZnO, and Al_2O_3 nanoparticles within the PS matrix remarkably enhances σ_{AC} compared to pure PS. The addition of nanofillers reduces the potential barrier height and shortens the inter-particle hopping distance between localized states in the band gap, creating continuous conductive percolation pathways through the polymer network. Across all samples, σ_{AC}increases steadily with increasing frequency due to the enhanced excitation and hopping of charge carriers between the valence and conduction bands. The enhancement in AC electrical conductivity follows the ascending order:

Pure PS < PS/ Al_2O_3 < PS/ ZrO_2 < PS/ ZnO < PS/ MnO_2

The PS/ $MnO_2$and PS/ ZnO films demonstrate the highest electrical conductivity owing to the narrow band gap and high electronic/ionic carrier mobility of PS/ MnO_2 and PS/ ZnO nanoparticles, whereas PS/ Al_2O_3 exhibits the lowest conductivity among the doped systems due to the wide band gap and insulating nature of PS/ Al_2O_3

3.4. Dielectric Loss Factor (tan *δ*)

The dielectric loss tangent (tan *δ*), which quantifies the phase lag and energy dissipation inside the dielectric medium under an alternating electric field, was calculated using Equation (5), figure (4) showen Dielectric loss factor (tan δ) of different PS nanocomposite films relationship with frequency at room temperature.

:

$$(\tan \delta)=\frac{\varepsilon''}{\varepsilon'}\text{.....(5)}$$

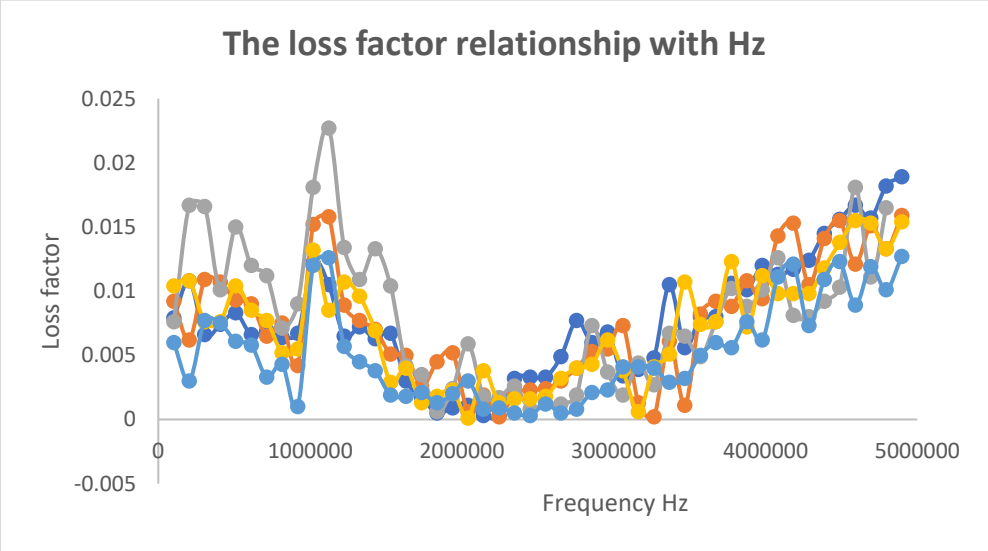


Figure 4. Dielectric loss factor (tan δ) of different PS nanocomposite films relationship with frequency at room temperature.

The applied frequency induces molecular vibrations in the PS chains, promoting dipolar relaxation and charge carrier transitions that govern energy dissipation. As frequency increases, (tan *δ*) decreases gradually across all samples because charge carriers and dipoles cannot respond instantaneously to rapid field reversals. Moreover, the incorporation of metal oxide nanoparticles effectively modulates the energy dissipation behavior, confirming that these nanofillers stabilize the dielectric response of the PS matrix for high-frequency electronic applications.

3.5. Surface and Volume Energy Loss Functions (SELF and VELF)

The surface energy loss function (SELF) and volume energy loss function (VELF) describe the rate of energy loss experienced by fast-moving electrons traversing the surface and bulk volume of the PS nanocomposite films, respectively. Both parameters are directly related to ε' and ε'' and were evaluated using Equations (6) and (7):

$$SELF = \frac{\varepsilon''}{(\varepsilon')^2 + (\varepsilon'')^2} \quad \ldots\ldots\ldots\ldots\ldots\ldots\ldots\ldots\ldots\ldots (6)$$

$$VELF = \frac{\varepsilon''}{(\varepsilon'+1)^2 + (\varepsilon'')^2} \quad \ldots\ldots\ldots\ldots\ldots\ldots\ldots\ldots\ldots\ldots (7)$$

Both SELF and VELF exhibit a gradual decline with increasing logarithmic frequency, mirroring the dispersion trends observed in ε' and ε''. The incorporation of ZrO_2, MnO_2, ZnO, and Al_2O_3 nanoparticles alters the electron scattering probabilities within the polymer lattice. Notably, SELF values remain consistently higher than VELF values across the (1-3 MHz) range, indicating that energy dissipation of free charge carriers is more pronounced at the film surface and interfacial boundaries than within the bulk volume of the PS matrix,figure (5) showen Surface energy loss factors relationship with frequency logarithm of different PS nanocomposite films at room temperature and figure (6) showen Volume energy loss factors relationship with frequency logarithm of different PVB nanocomposite films at room temperature.

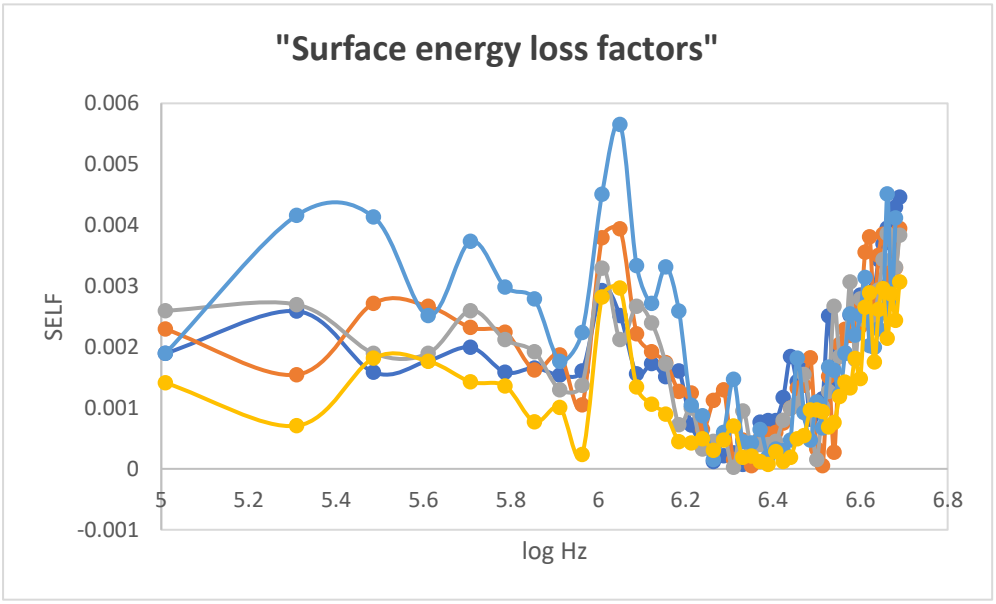


Figure 5. SELF relationship with frequency logarithm of different PS nanocomposite films at room temperature.

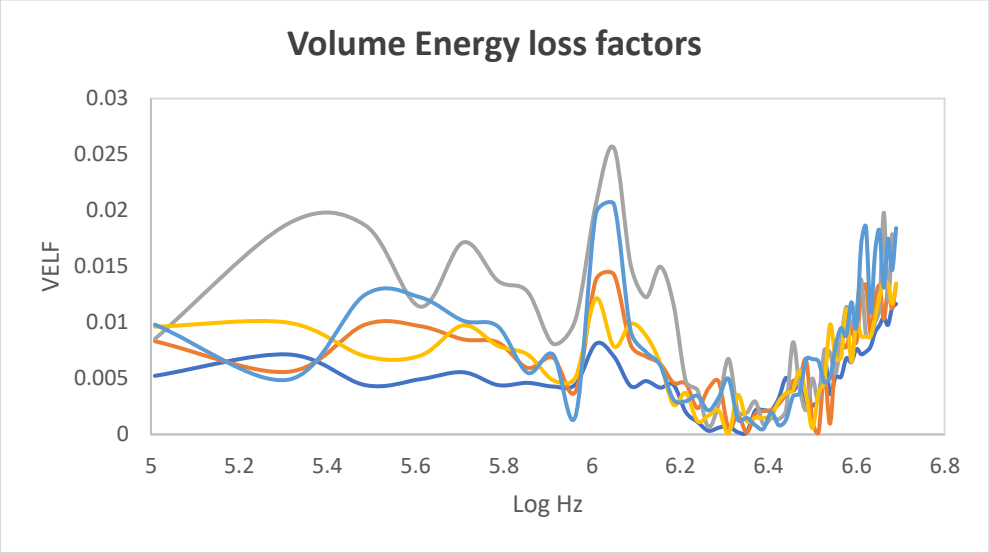


Figure 6. VELF relationship with frequency logarithm of different PVB nanocomposite films at room temperature.

3.6. FESEM and Optical Microscopy Analysis

The surface morphological features of the blank PS and PS nanocomposite films were examined using field emission scanning electron microscopy (FESEM) at an accelerating voltage of 10kV and optical microscopy at 400× magnification. The blank PS film displays a relatively smooth, uniform, and homogeneous surface typical of an amorphous thermoplastic polymer. Upon doping with 0.005 wt.% of ZrO_2 , MnO_2, ZnO, and Al_2O_3 nanoparticles, distinct morphological transformations appear across the film surfaces, characterized by increased surface roughness, micro-troughs, and well-dispersed bright nano-domains. Each metal oxide imparts a unique surface texture depending on its particle size and interfacial compatibility with the hydrophobic phenyl rings of PS. Optical microscopy images further corroborate these structural modifications, revealing granular textures and light-scattering regions induced by the embedded nanofillers.

3.7. EDX Elemental Analysis

EDX spectroscopy was employed as an effective technique to obtain the elemental spectrum of the polystyrene (PS) film, as shown in Figure 8. From the spectrum, a homogeneous distribution of elements across the pure PS polymer matrix can be recognized [9, 10]. However, changes in the films' composition and morphology can be observed after incorporating the nanoparticles (ZrO_2, MnO_2, ZnO, and Al_2O_3), resulting in altered properties [11–13]. It is evident from the EDX analysis that all constituent elements appeared as distinct peaks in both the pure PS and metal-oxide-doped PS samples. Energy-dispersive X-ray (EDX) spectroscopy was conducted on the polystyrene (PS) nanocomposite films doped with ZrO_2, MnO_2, ZnO, and Al_2O_3 , as shown in Figures (7) , respectively. The spectra confirm the successful incorporation and dispersion of the metal oxide nanoparticles (NPs) within the PS polymer matrix across varying concentrations [14, 15]. Specifically, the EDX elemental profiles reveal the emergence of distinct characteristic peaks at 2.04, 8.64, 1.49, and 5.90 keV, corresponding to Zr Lα , Zn Kα, Al Kα), and Mn K α) in the respective nanocomposites Figures (8)). Although standard EDX analysis provides semi-quantitative rather than absolute quantitative data, it offers valuable insight into the near-surface elemental composition of the films. Notably, the oxygen peak intensity (0.525 keV) increases significantly compared to that of the pure PS polymer, which is directly attributed to the additional oxygen introduced by the metal oxide nanofillers [16].

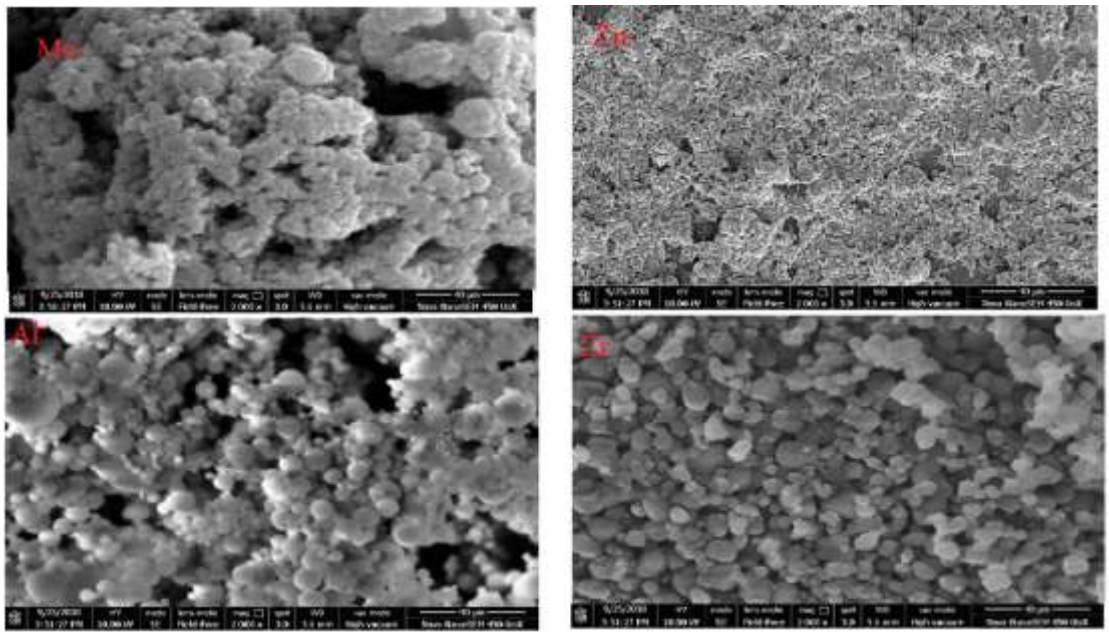


Figure 7. FESEM images of nanocomposite PS films.

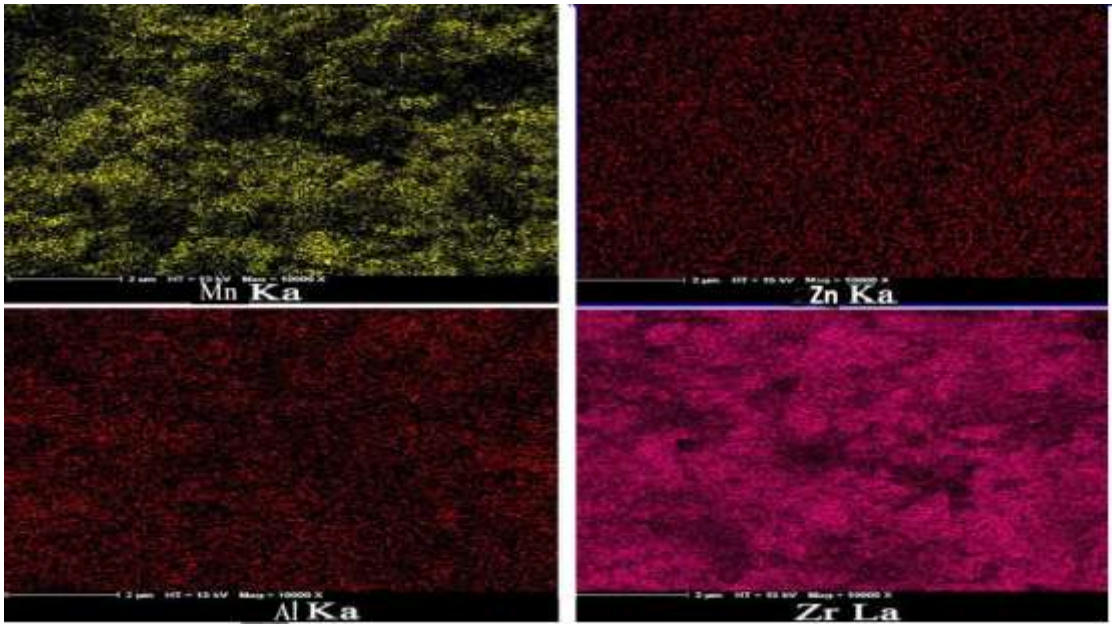


Figure 8. Microscope images of nanocomposite PS films with 400X magnification.

4. Conclusion

Polystyrene (PS) nanocomposite films doped with 0.005 wt. % of ZrO_2, MnO_2, ZnO, and Al_2O_3 nanoparticles were successfully synthesized via the solution casting method. The electrical and dielectric properties of the fabricated films were systematically evaluated across the frequency range of (1-3 MHz) at room temperature. Incorporating the metal oxide nanofillers significantly enhanced the real and imaginary dielectric constants (ἐ and ε'') and AC electrical conductivity (σ_{AC}) compared to the blank PS film. Among the investigated composites, PS/MnO_2 and PS/ZnO achieved the highest electrical conductivity due to enhanced charge carrier hopping and interfacial polarization, whereas PS/ZrO_2 demonstrated superior dielectric permittivity. Conversely, the dielectric loss factor (tan δ), surface energy loss function (SELF), and volume energy loss function (VELF) decreased progressively with increasing frequency. FESEM and optical microscopy observations confirmed uniform nanoparticle dispersion and increased surface roughness upon doping, while EDX spectra verified the presence of Zr, Mn , Zn, Al, and O elements

within the PS matrix. Overall, these findings demonstrate that doping PS with trace amounts of metal oxide nanoparticles effectively tailors its electrical and morphological properties, rendering these nanocomposite films promising candidates for microelectronic capacitors, optoelectronic devices, and dielectric coatings.

REFERENCES

[1] E. Yousif, D. S. Ahmed, G. A. El-Hiti, M. H. Alotaibi, H. Hashim, and A. S. Hameed, "Fabrication of novel polystyrene composites containing metal oxide nanoparticles: Surface morphology and photostability," *Polymers*, vol. 11, no. 6, Art. no. 982, 2019.

[2] E. Al-Bermany and B. Chen, "Preparation and characterisation of poly(styrene)/graphene oxide nanocomposites," *Polymer International*, vol. 63, no. 10, pp. 1791–1800, 2014.

[3] A. M. Abdul-Kader, N. A. El-Ghamaz, and R. M. El-Shazly, "Effect of metal oxide nanoparticles on the AC conductivity and dielectric relaxation of polystyrene films," *Physica B: Condensed Matter*, vol. 546, pp. 25–32, 2018.

[4] R. J. Sengwa and P. Dhatarwal, "Predominantly chain segmental relaxation dependent ionic conductivity and dielectric properties of metal oxide nanoparticles filled polymer nanocomposites," *Electrochimica Acta*, vol. 338, Art. no. 135890, 2020.

[5] R. K. Goyal and A. Saini, "Dielectric and thermal properties of polystyrene/ZrO2 nanocomposites prepared by solution casting method," *Journal of Electronic Materials*, vol. 47, no. 3, pp. 1890–1897, 2018.

[6] N. A. El-Ghamaz, R. M. El-Shazly, and A. M. Abdul-Kader, "Structural, optical, and AC electrical conductivity of polystyrene doped with MnO2 nanoparticles," *Journal of Materials Science: Materials in Electronics*, vol. 30, no. 14, pp. 13245–13254, 2019.

[7] S. Choudhary and R. J. Sengwa, "Dielectric spectroscopy and structural characterization of ZnO nanoparticles dispersed polystyrene nanocomposites," *Journal of Applied Polymer Science*, vol. 134, no. 11, Art. no. 44568, 2017.

[8] A. H. Majeed and H. A. Al-Attar, "Structural, optical and electrical properties of polystyrene doped with Al2O3 nanoparticles," *Materials Research Express*, vol. 6, no. 8, Art. no. 085312, 2019.

[9] S. Dey, D. Mohan, G. C. Dhal, and R. Prasad, "Copper based mixed oxide catalysts (CuMnCe, CuMnCo and CuCeZr) for the oxidation of CO at low temperature," *Materials Discovery*, vol. 10, pp. 1–14, 2017, doi: 10.1016/j.md.2018.02.001.

[10] R. Divya, M. Meena, C. K. Mahadevan, and C. M. Padma, "Investigation on CuO dispersed PVA polymer films," *International Journal of Engineering Research and Applications*, vol. 4, pp. 1–7, 2014.

[11] P. Kumar, N. Khan, and D. Kumar, "Polyvinyl butyral (PVB), versatile template for designing nanocomposite/composite materials: A review," *Green Chemistry and Technology Letters*, vol. 2, no. 4, pp. 185–194, 2016, doi: 10.18510/gctl.2016.244.

[12] H. E. Atyia and N. A. Hegab, "Determination and analysis of optical constants for Ge15Se60Bi25 thin films," *Physica B: Condensed Matter*, vol. 454, pp. 189–196, 2014, doi: 10.1016/j.physb.2014.07.068.

[13] T. Niratiwongkorn, G. E. Luckachan, and V. Mittal, "Self-healing protective coatings of polyvinyl butyral/polypyrrole-carbon black composite on carbon steel," *RSC Advances*, vol. 6, pp. 43237–43249, 2016, doi: 10.1039/C6RA01619G.

[14] S. Dey and G. C. Dhal, "Property and structure of various platinum catalysts for low-temperature carbon monoxide oxidations," *Materials Today Chemistry*, vol. 16, Art. no. 100228, 2020, doi: 10.1016/j.mtchem.2019.100228.

[15] S. Dey, G. C. Dhal, D. Mohan, and R. Prasad, "Structural and catalytic properties of Fe and Ni doping on CuMnOx catalyst for CO oxidation," *Advanced Composites and Hybrid Materials*, vol. 3, pp. 84–97, 2020, doi: 10.1007/s42114-020-00139-3.

[16] M. B. Povea, W. A. Monal, J. V. C. Rodríguez, A. M. Pat, N. B. Rivero, and C. P. Covas, "Interpenetrated chitosan-poly(acrylic acid-co-acrylamide) hydrogels: Synthesis, characterization and sustained protein release studies," *Materials Sciences and Applications*, vol. 2, pp. 509–520, 2011, doi: 10.4236/msa.2011.26069.